processes

MDPI

Article

Influence of Hydrothermal Pretreatment Temperature on the Hydration Properties and Direct Carbonation Efficiency of Al-Rich Ladle Furnace Refining Slag

Yi Huang [1,*] and Guo Xiong [2]

[1] School of Materials and Chemical Engineering, Hunan City University, Yiyang 413002, China
[2] Hunan Hualin Xiangtan Iron and Steel Co., Ltd., Xiangtan 411101, China; xgsz50@163.com
* Correspondence: Huangyi@hncu.edu.cn

Abstract: The influence of hydrothermal pretreatment temperature on the hydration products and carbonation efficiency of Al-rich LF slag was investigated. The results showed that the carbonation efficiency was strongly dependent on the morphology of hydration products and the hydration extent of the raw slag. Hydrothermal pretreatment at 20 °C or 80 °C favored the formation of flake-shaped products with a higher specific surface area and therefore resulted in a higher CO_2 uptake of 20 °C and 80 °C-pretreated slags (13.66 wt% and 10.82 wt%, respectively). However, hydrothermal pretreatment at 40 °C, 60 °C or 100 °C led to the rhombohedral-shaped calcite layer surrounding the unreacted core of the raw slag and the formation of fewer flake-shaped products, resulting in a lower CO_2 uptake of 40 °C, 60 °C and 100 °C-pretreated slags (9.21 wt%, 9.83 wt%, and 6.84 wt%, respectively).

Keywords: LF slag; hydrothermal pretreatment; temperature; hydration products; CO_2 uptake

Citation: Huang, Y.; Xiong, G. Influence of Hydrothermal Pretreatment Temperature on the Hydration Properties and Direct Carbonation Efficiency of Al-Rich Ladle Furnace Refining Slag. *Processes* **2021**, *9*, 1458. https://doi.org/10.3390/pr9081458

Academic Editor: Federica Raganati

Received: 29 July 2021
Accepted: 19 August 2021
Published: 21 August 2021

1. Introduction

The growth of global greenhouse gas emissions was 2.0% in 2018 and there is no sign that any of these emissions are peaking yet. The six largest emitters of greenhouse gases, together accounting for 62% globally, are China (26%), the United States (13%), the European Union (more than 8%), India (7%), the Russian Federation (5%), and Japan (almost 3%) [1]. China's carbon emission peak is a matter of international focus. Recently, China made a solemn promise to peak its carbon dioxide emission by 2030 and achieve carbon neutrality by 2060. Some of the main measures China will use to reduce CO_2 emissions over next 10 years are: changing energy and industrial structures, transforming the development mode, promoting clean energy, and appropriately increasing carbon sequestration ability. Among the current CO_2 sequestration routes, mineral carbonation is regarded as a potential technology because of its advantages; it is environmentally benign, it enables the permanent trapping of CO_2 in the form of carbonate, and it does not require post-storage surveillance for CO_2 leakage [2]. In general, mineral carbonation can be divided into two categories, namely direct carbonation and indirect carbonation. Direct mineral carbonation is accomplished through the reaction of a solid alkaline mineral with CO_2, either in gaseous or in aqueous phase [3].

Alkaline solid wastes such as red mud, steel slag, blast furnace slag, fly ash, etc., are used for direct mineral carbonation as efficient and economically available capturers of CO_2 [4–9]. For the direct mineral carbonation of steel slag, the formation of an increasingly thick and dense carbonate layer surrounding the unreacted core of the solid particle hinders further carbonation and results in the lower CO_2 capture capacity [10]. In our previous study [11], the improvement in the direct carbonation efficiency of Al-rich ladle furnace refining slag (LF slag) by hydrothermal pretreatment was investigated. The results showed that after hydrothermal pretreatment at 80 °C, the morphology of $Ca_{12}Al_{14}O_{33}$($C_{12}A_7$) in

the slag transformed from separated particles to the flake-shaped $Ca_3Al_2O_6{\cdot}xH_2O(C_3AH_x)$, resulting in an increased reaction surface area and carbonation efficiency. However, this study did not discuss the effect of hydrothermal temperature on the carbonation efficiency. In fact, the hydration product of $C_{12}A_7$ is dependent on the hydration temperature. Koplík et al. [12] reported that at 20 °C the major hydration products of $C_{12}A_7$ were $Ca_2Al_2O_5{\cdot}8H_2O(C_2AH_8)$ and $CaAl_2O_4{\cdot}10H_2O(CAH_{10})$; at 30 °C CAH_{10} disappeared and only C_2AH_8 remained; at 60 °C the only stable hydrates–$Ca_3Al_2O_6{\cdot}6H_2O(C_3AH_6)$ and $Al(OH)_3$(AH) were formed. Edmonds et al. [13] stated that both C_2AH_8 and CAH_{10} can be produced during the hydration of $C_{12}A_7$ at 4 °C, while no trace of CAH_{10} was spotted when $C_{12}A_7$ was hydrated at 20 or 40 °C. Given that the morphology of the hydration product of C12A7 has a significant effect on the carbonation efficiency of LF slag and the type of hydration product produced is related to temperature, the aim of this study was to investigate the influence of hydrothermal pre-treatment temperature on the hydration properties and the carbonation efficiency of Al-rich LF slag at ambient temperature and pressure. Moreover, the relation between the morphology of the hydration product and the carbonation efficiency was clarified in this work.

2. Materials and Methods

2.1. Materials

The Al-rich LF slag used in this study was collected from the Xiangtan steel plant in Hunan province, China. The chemical composition of the slag determined by X-ray Fluorescence (XRF) is listed in Table 1. Before pretreatment, the raw slag was crushed and ground into a powder <20 mesh particle size. Distilled water was used in this study for slag suspension preparation.

Table 1. Chemical composition of raw slag as determined by XRF analysis.

Component	CaO	Al_2O_3	SiO_2	MgO	TiO_2	SO_3	Fe_2O_3	Others
wt%	52.0056	23.66	15.83	4.05	0.90	2.45	0.54	0.57

2.2. Hydrothermal Pretreatment of LF Slag at Different Temperatures

At first, the raw slag was fully mixed with water at a solid/water (*S*/*W*) ratio of 1:10 in a beaker. Then, the suspension was stirred for 30 min at 20, 40, 60, 80 and 100 °C (designated as 20H, 40H, 60H, 80H and 100H-slag, respectively). Next, the suspension was filtered and the obtained solid was sufficiently washed and dried to a constant weight at 105 °C for further characterization and for the following carbonation experiment.

2.3. Direct Aqueous Carbonation Process

The schematic diagram of the aqueous carbonation experimental system is shown in Figure 1. The pretreated slag suspension with a solid/water ratio of 1:10 was placed in a conical flask into an electric-heated thermostatic water bath equipped with a mechanical stirrer. The temperature of the water bath was kept at 40 °C. Then, 99.99% pure CO_2 from the CO_2 cylinder was injected into the suspension at a flow rate of 5 L/min controlled by a flowmeter, and was simultaneously stirred for carbonation. The suspension underwent the carbonation process for 60 min and was then filtered. The obtained solid was dried to a constant weight at 105 °C for further characterization.

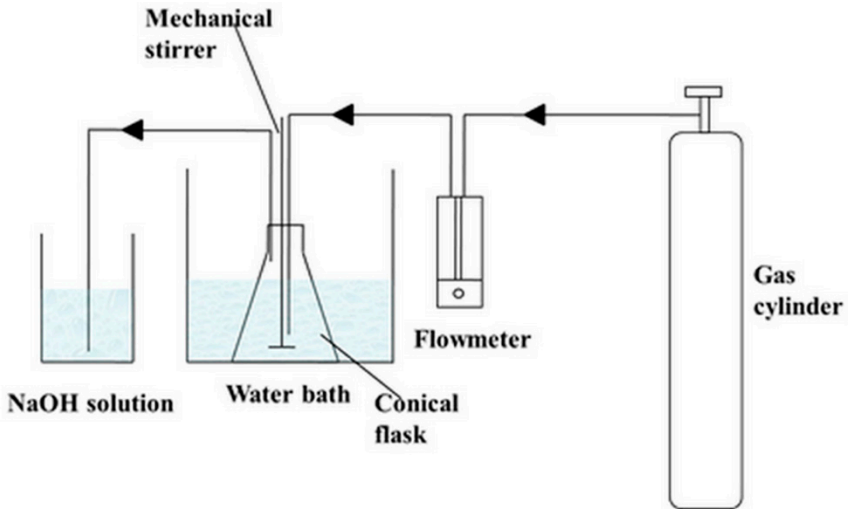

Figure 1. Schematic diagram of the aqueous carbonation experimental system.

2.4. Characterization of Slag

X-ray diffraction (XRD, Bruker AXS company D8 Advance, Karlsruhe, Germany) was conducted on the slags to identify their main mineral phases. The scanning range was from 5° to 70° 2θ at 2°/min. TG-DSC analysis was performed using a METTLER TOLEDO 1600 LF thermal gravimetric analyzer. A field-emission scanning electron microscope (FESEM, Hitachi company SU8010, Tokyo, Japan) was used to characterize the morphology of the slag. The specific surface area of the slags was measured by the N_2 gas adsorption Brunauer–Emmet–Teller (BET) method (ASAP 2020, Micromeritics, Norcross, GA, USA). The pH value of the slag suspension was determined by a PHS-3C pH meter.

2.5. Analysis of Carbonation Efficiency

In order to compare the carbonation efficiency of Al-rich LF slags under the hydrothermal pretreatment at different temperatures, the CO_2 uptake of the slags was measured based on the weight fraction of the TG curve ($\Delta m_{600–800\,^{\circ}C}$) and the dry weight (m) [14] expressed in terms of CO_2 (wt%), Equation (1):

$$CO_2(wt\%) = \frac{\Delta m_{600–800\,^{\circ}C}}{m} \times 100 \quad (1)$$

3. Results and Discussion

3.1. Influence of Hydrothermal Temperature on Hydration Properties of Al-Rich LF Slag

Figure 2 shows the XRD patterns of the raw slag and the pretreated slags. The main mineral phases of raw slag were $C_{12}A_7$ and $Ca_2SiO_4(CS_2)$. For all the slags with pretreatment, the peaks of $C_{12}A_7$ were reduced, indicating its hydration. The 40H-slag and 100H-slag presented relatively more intense residual $C_{12}A_7$ peaks than the other slags, suggesting the lower hydration extent of these two slags. For the 20H-slag, $3CaO{\cdot}Al_2O_3{\cdot}CaCO_3{\cdot}11H_2O(C_4A\overline{C}H_{11})$ was the dominant hydration product. A small amount of ($C_4A\overline{C}H_{11}$) also appeared in the 40H-slag and C_3AH_6 was the other main product for this slag. Hydrocalumite ($Ca_4Al_2(OH)_{12}CO_3{\cdot}5H_2O$) was only present in the 100H-slag, and this slag had the most intense C_3AH_6 peaks. With respect to the 60H-slag, only C_3AH_6 crystal was found. In general, C_3AHx, $C_4A\overline{C}H_{11}$, and C_3AH_6 were the main hydration products, while the other products mentioned in the "Introduction" (such as CAH_{10} and C_2AH_8) were not observed. This could be explained by the fact that CAH_{10} and C_2AH_8 are the transition phases and can be converted to the ultimate stable products (e.g., C_3AH_6 and C_3AH_x), described by Equations (2)–(4), respectively [15].

$$2CAH_{10} \rightarrow C_2AH_8 + AH_3 + 9H \quad (2)$$

$$3C_2AH_8 \rightarrow 2C_3AH_6 + AH_3 + 9H \quad (3)$$

$$3C_2AH_8 \rightarrow 2C_3AH_x + AH_3 + (21 - 2x)H \quad (4)$$

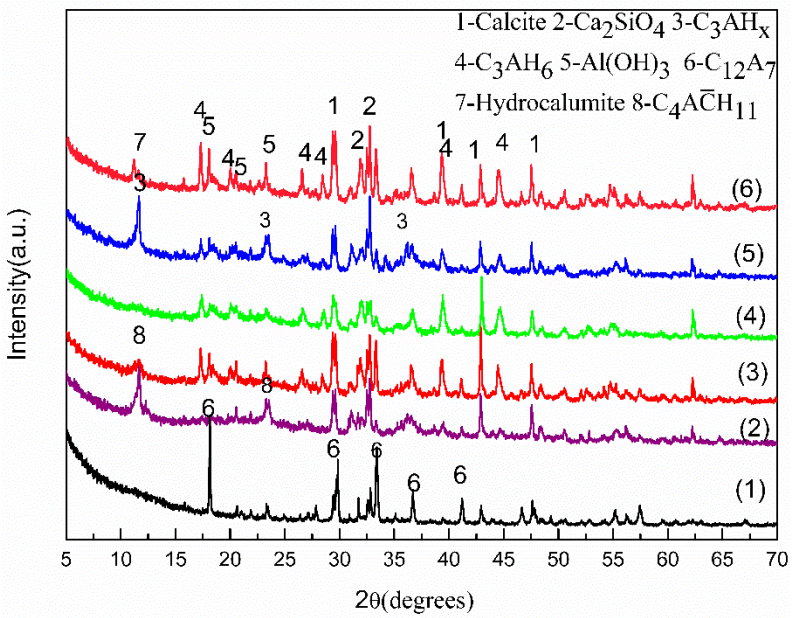

Figure 2. XRD patterns of (1) raw slag, (2) 20H-slag, (3) 40H-slag, (4) 60H-slag, (5) 80H-slag, and (6) 100H-slag.

Figure 3 displays the FESEM pictures of the raw slag and the pretreated slags. The raw slag appeared as irregular-shaped particles with dense and coarse surfaces (Figure 3a). After hydration at 20 °C, the slag surface became smooth due to the formation of flake-shaped $C_4A\bar{C}H_{11}$ (Figure 3b). In addition, metastable hydrates in the form of hexagonal platelets [14] were observed (Figure 3b). The microstructure of the 40H-slag presented as a mixture of $C_4A\bar{C}H_{11}$, metastable hydrated hexagonal-shaped platelets [16], and unhydrated slag particles (Figure 3c). The edge of the unhydrated particles in the 40H-slag was covered by rhombohedral-shaped $CaCO_3$ (calcite) particles and AH gel with a grain size of 0.5 μm, which may hinder the further hydration of $C_{12}A_7$ (Figure 3d). Once again, this verified that the thick and dense $CaCO_3$ layer surrounding the unreacted core of the solid particle was the main cause of the low carbonation efficiency of the slag without hydrothermal pretreatment, as illustrated in our previous studies [9]. $CaCO_3$ and AH gel should be generated by the indirect carbonation reaction between $C_{12}A_7$ and CO_2 in the air, which can be described by Equations (5) and (6) [17]. The occurrence of Equation (5) resulted in the alkalinity of the slag suspensions (the final pH values were 10.42, 10.13, 10.05, 10.56, and 10.02 for the slag suspensions treated at 20 °C, 40 °C, 60 °C, 80 °C, and 100 °C, respectively).

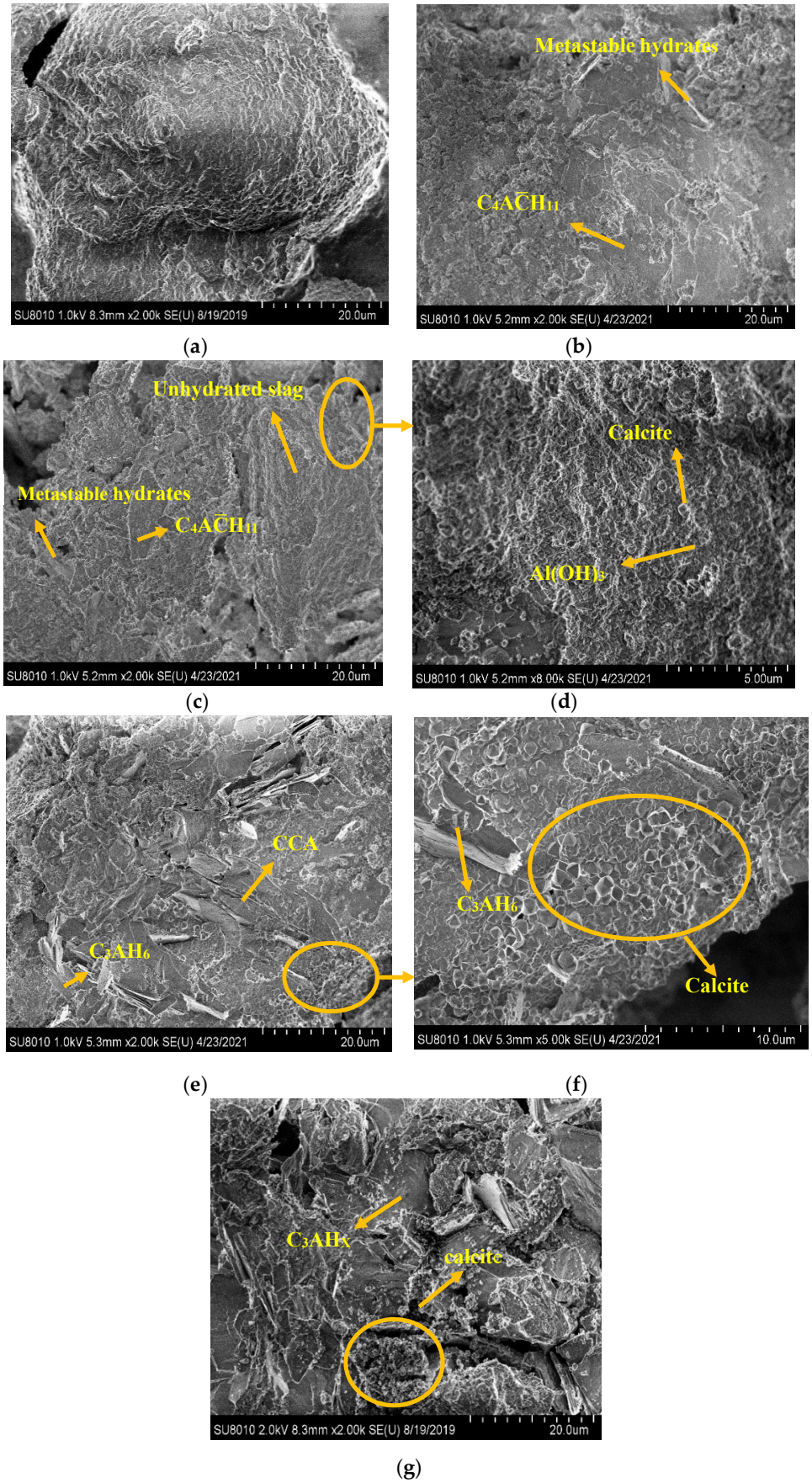

Figure 3. *Cont.*

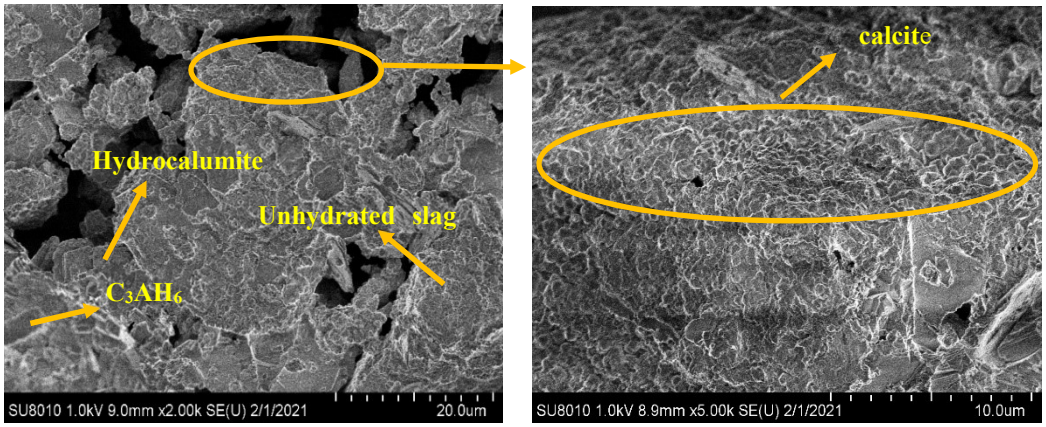

(**h**) (**i**)

Figure 3. FESEM pictures of (**a**) raw slag 2000×, (**b**) 20H-slag 2000×, (**c**) 40H-slag 2000×, (**d**) 40H-slag 8000×, (**e**) 60H-slag 2000×, (**f**) 60H-slag 5000×, (**g**) 80H slag 2000×, (**h**) 100H-slag 2000× and (**i**) 100H-slag 5000×.

The FESEM image of the 60H-slag (Figure 3e) indicates the formation of flake-shaped and cubic hydrates that should be amorphous calcium carboaluminate (CCA) and C_3AH_6, respectively. In addition, a dense rhombohedral-shaped calcite layer covered part of the slag surface (Figure 3f). Therefore, it is assumed that CCA was formed through the reaction between C_3AH_6 and calcite [18,19]. This also provides an explanation for why the 20H-slag contained large amounts of $C_4A\overline{C}H_{11}$ but small amounts of calcite formation (the reaction between C_3AH_6 and calcite can be described by Equation (7) [19]). After hydration at 80 °C, the morphology of the slag changed from separated particles to continuous gel (Figure 3g). The flake-shaped gel should be C_3AH_x, and calcite particles were scattered on the surface of C_3AH_X in the 80H-slag (Figure 3g). For the 100H-slag, flake-shaped hydrocalumite and cubic C_3AH_6 particles were embedded in the unhydrated slag particles (Figure 3h), and a rhombohedral-shaped calcite layer deposited on the edge of the slag particles (Figure 3i), similarly to the 40H and 60H slag.

$$Ca_{12}Al_{14}O_{33} + 33H_2O \rightarrow 12Ca^{2+} + 14Al(OH)_4^- + 10OH^- \quad (5)$$

$$Ca^{2+} + CO_2 + 2Al(OH)_4^- \rightarrow CaCO_3\downarrow + 2Al(OH)_3\downarrow + H_2O \quad (6)$$

$$CaCO_3 + Ca_3Al_2O_6{\cdot}6H_2O + 5H_2O \rightarrow 3CaO{\cdot}Al_2O_3{\cdot}CaCO_3{\cdot}11H_2O \quad (7)$$

The BET specific surface area (S_{BET}) of the slags were listed in Table 2. The S_{BET} of the 20H-slag and the 80H-slag was more than two times that of the raw slag, while other pretreated slags demonstrated only a slight S_{BET} increase compared with the raw slag. This should be attributed to the larger amount of flake-shaped hydrates in the 20H-slag and the 80H-slag [20].

Table 2. The BET specific surface area of the pretreated slags.

	Raw Slag	20H-Slag	40H-Slag	60H-Slag	80H-Slag	100H-Slag
SBET (m^2/g)	4.68	8.32	5.89	6.15	9.40	5.15

Figure 4 shows the TG-DSC analysis results of the pretreated slags. The endothermic peak of around 260–270 °C denoted the decomposition of $Al(OH)_3$ and appeared in all slags [19]. This peak was overlapped by the endothermic peak between 280 °C and 325 °C, which was attributed to the dehydration of C_3AH_6 in the 40H-slag, 60H-slag,

and 80H-slag [18]. These results corresponded well with the XRD and FESEM analysis. The endothermic peak at 157 °C in the 20H-salg indicated the dehydration of $C_4A\overline{C}H_{11}$ [16], while this peak became broad for the 40H-slag due to the low crystallinity of $C_4A\overline{C}H_{11}$ [16], as was also reflected in the broad peak of XRD patterns (Figure 1). The absence of $C_4A\overline{C}H_{11}$ in the other slags can be explained by its instability in temperatures above 40 °C [19]. A very broad endothermic peak between 80 and 200 °C was observed in the 60H-slag, generated by the dehydration of amorphous CCA [14]. The endothermic peak at 155 °C in the 80H-slag represented the dehydration of C_3AH_x which is close to the dehydration temperatures of CAH_{10} and C_2AH_8 [15]. With respect to the 100H-slag, the dehydration of hydrocalumite was reflected in the endothermic peak around 146 °C. In general, the dehydration of hydrates mainly occurred over the temperature range of 105–325 °C, resulting in significant weight loss. The other significant weight loss region was between 600 and 800 °C, which was ascribed to the $CaCO_3$ decomposition. During the hydrothermal process, $C_{12}A_7$ was transformed into calcium aluminates hydrate (CAH), CAC, AH, and $CaCO_3$; therefore, the mass loss ratio of the slags (See Table 3) above the temperature range of 105–800 °C should be an indicator of $C_{12}A_7$ hydration extent. It may be concluded from the results in Table 2 that the 20H-slag and the 80H-slag had significantly higher hydration extent than other three slags, in good agreement with the XRD and FESEM analysis.

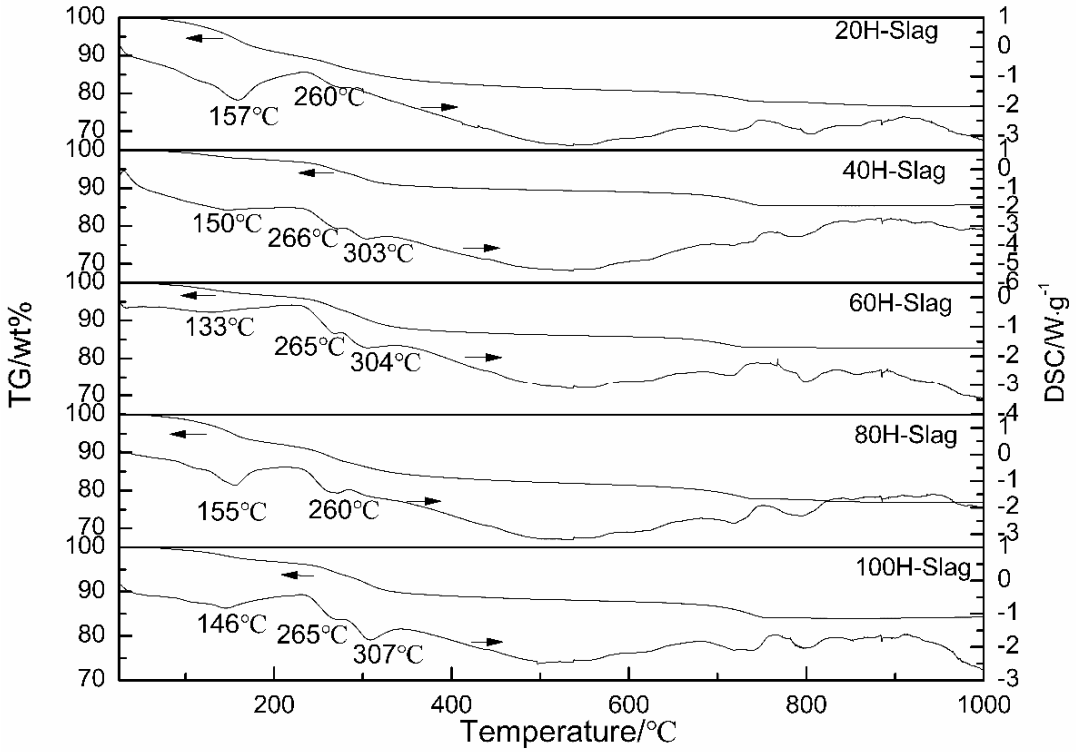

Figure 4. TG-DSC curves of the pretreated slags.

Table 3. The mass loss ratio of the pretreated slags between 105 and 800 °C.

Sample	Mass Loss Ratio between 105 and 800 °C (wt%)
20H-slag	20.58
40H-slag	13.80
60H-slag	15.95
80H-slag	20.70
100H-slag	15.07

In conclusion, cubic C_3AH_6 was a main hydration product for the 40H-slag, 60H-slag, and 100H-slag. Part of C_3AH_6 could react with $CaCO_3$ to generate CCA while the unreacted

rhombohedral-shaped $CaCO_3$ layer covered the slag surface, resulting in the hindrance of further hydration for these three slags. By contrast, flake-shaped $C_4A\overline{C}H_{11}$ and C_3AH_x were the main hydration products for the 20H-slag and the 80H-slag, respectively, and their higher specific surface area may accelerate the carbonation reaction.

3.2. Carbonation Efficiency of Slags Pretreated at Different Temperatures

The XRD patterns of the slags after carbonation are shown in Figure 5. After carbonation, the peaks of C_3AH_x, $C_4A\overline{C}H_{11}$, and hydrocalumite disappeared or showed a significant decrease in intensity while the calcite peaks increased in intensity. This suggests the carbonation of these hydrates. On the contrary, C_3AH_6 appeared less active in terms of its carbonation, which may be the main cause of the less intense calcite peaks in the carbonated100H-slag with C_3AH_6 as the main hydration product (see Figure 1). In addition, residual $C_4A\overline{C}H_{11}$ peaks were observed, indicating the incomplete carbonation of $C_4A\overline{C}H_{11}$ in the 20H-slag during carbonation. This resulted in the less intense calcite peaks in the carbonated 20H-slag compared with the carbonated 80H-slag.

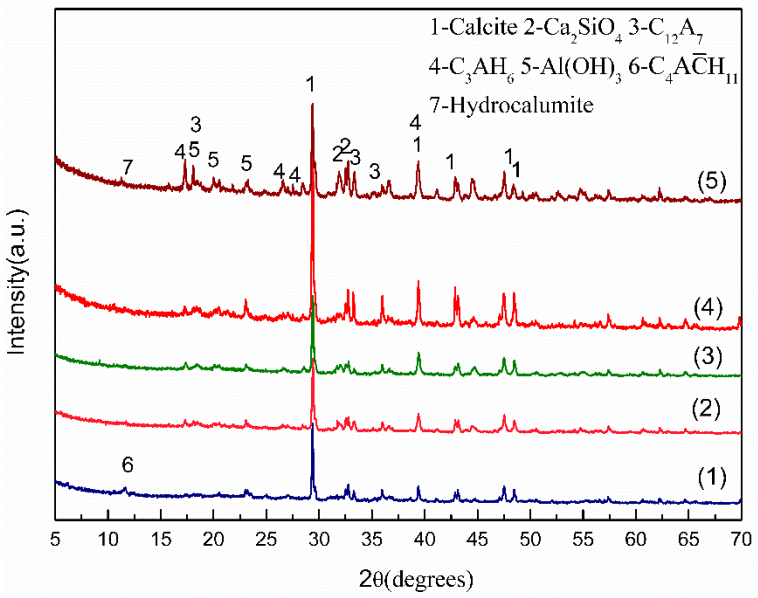

Figure 5. XRD patterns of (1) carbonated 20H-slag, (2) carbonated 40H-slag, (3) carbonated 60H-slag, (4) carbonated 80H-slag, and (5) carbonated 100H-slag.

Figure 6 exhibits the FESEM pictures of the slags after carbonation. For the carbonated 20H-slag, flake-shaped $C_4A\overline{C}H_{11}$ was decomposed and cubic calcite crystals were observable (Figure 6a). In the carbonated 40H-slag and 60H-slag, some of the cubic calcite crystals were surrounded by unreacted hydrates (Figure 6b,c). Larger amounts of cubic calcite crystals appeared in the carbonated 80H-slag than in the other slags, leading to the breakdown of continuous C_3AH_x gel (Figure 6d). Moreover, the carbonation products were covered by a small amount of unreacted C_3AH_x debris (Figure 6d). The microstructure of the carbonated 100H-slag (Figure 6e) was similar to the carbonated 40H-slag and 60H-slag; it was composed of unreacted hydration products, unhydrated slag, and some cubic calcite crystals. In each of the slags, the cubic calcite was generated by the direct reaction of CO_2 with the hydrates and amorphous AH, as the other reaction product surrounded the cubic calcite crystals [11]. In each of the carbonated slags, calcite appeared as non-uniform aggregated crystal particles, which indicate direct carbonation [21]. Direct carbonation of alkaline slag involved two stages: CO_2 dissolution and carbonation reaction [21,22]. The simplified direct carbonation mechanism of slags with hydrothermal pretreatment in this study was summarized in Table 4.

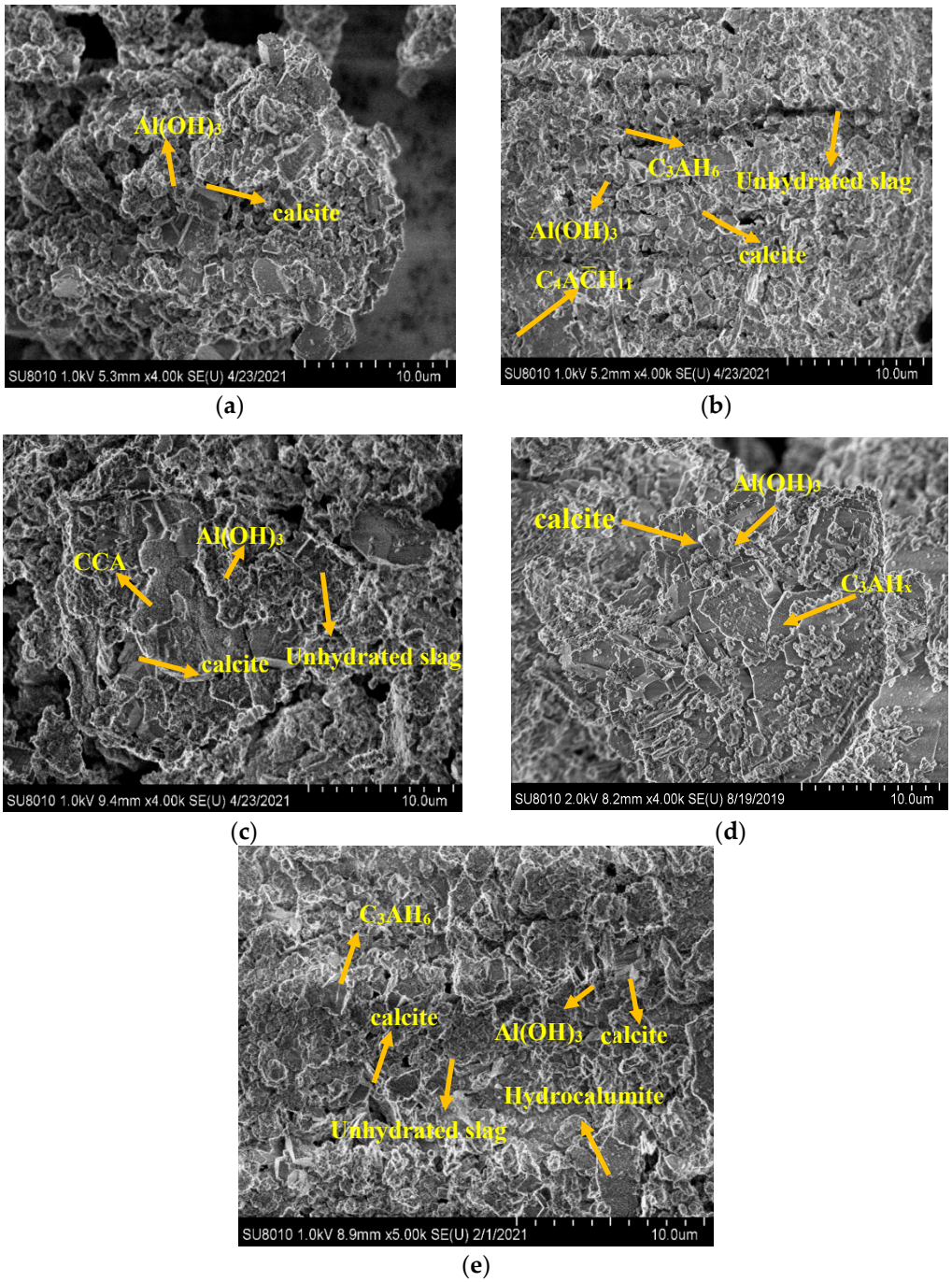

Figure 6. FESEM pictures of (**a**) carbonated 20H-slag, (**b**) carbonated 40H-slag, (**c**) carbonated 60H-slag, (**d**) carbonated 80H-slag, and (**e**) carbonated 100H-slag.

Table 4. Chemical reaction equations of the direct carbonation of the pretreated slags in this study.

Stage	Chemical Reaction Equation
CO_2 dissolution	$CO_{2(g)} \rightarrow CO_{2(aq)}$ $CO_{2(aq)} + 2OH^-{}_{(aq)} \rightarrow {CO_3}^{2-}{}_{(aq)} + H_2O_{(l)}$
Carbonation	$Ca_3Al_2O_6 \cdot 6H_2O_{(s)} + 3{CO_3}^{2-}{}_{(aq)} \rightarrow 3CaCO_{3(s)} + 2Al(OH)_{3(s)} + 6OH^-{}_{(aq)}$ $Ca_3Al_2O_6 \cdot xH_2O_{(s)} + 3{CO_3}^{2-}{}_{(aq)} \rightarrow 3CaCO_{3(s)} + 2Al(OH)_{3(s)} + 6OH^-{}_{(aq)} + (x-6)H_2O(l)$ $3CaO \cdot Al_2O_3 \cdot CaCO_3 \cdot 11H_2O_{(s)} + 3{CO_3}^{2-}{}_{(aq)} \rightarrow 4CaCO_{3(s)} + 2Al(OH)_{3(s)} + 6OH^-{}_{(aq)} + 5H_2O(l)$

Based on the TG curves of the carbonated slags (Figure 7), CO_2 uptake (wt%) was calculated with Equation (1) where m was the dry weight at 325 °C (at this temperature, free water and chemically bound water evaporated). The results of CO_2 uptake were listed in Table 5. The CO_2 uptake of slags followed this order: 80H-slag (13.66 wt%) > 20H-slag (10.82 wt%) > 60H-slag (9.83 wt%) > 40H-slag (9.21 wt%) > 100H-slag (6.84 wt%), which corresponded well with the XRD and FESEM results. This is attributed to the following reasons: (1) a dense $CaCO_3$ or AH gel layer covered the unhydrated slag surface in the 40H-slag and the 60H-slag, therefore resulting in the hindrance of further hydration and carbonation; (2) flake-shaped hydrates such as $C_4A\overline{C}H_{11}$ in the 20H-slag or C_3AH_x in the 80H-slag provided a larger reaction surface aera than the cubic C_3AH_6 and raw slag particles, avoiding calcite and AH gel layer formation on the unreacted hydrates surface. In short, the carbonation efficiency was strongly dependent on the type and morphology of the hydrates of LF slag.

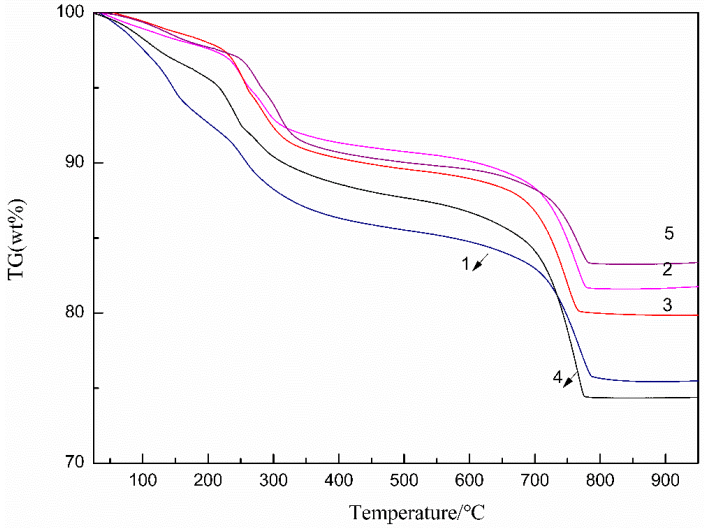

Figure 7. TG curves of (1) carbonated 20H-slag, (2) carbonated 40H-slag, (3) carbonated 60H-slag, (4) carbonated 80H-slag, and (5) carbonated 100H-slag.

Table 5. CO_2 uptake of pretreated slags.

	20H-Slag	40H-Slag	60H-Slag	80H-Slag	100H-Slag
CO_2 Uptake(wt%)	10.82	9.21	9.83	13.66	6.84

The maximum CO_2 uptake among these five pretreated slags was 13.66 wt% (namely 136.6 g of CO_2/1 kg of slag) which was attained by the 80H-slag. Compared with previous studies about wet direct carbonation of steelmaking slags conducted under ambient temperature and pressure (See Table 6), the CO_2 uptake of the 80H-slag in this study was considerable and the process was attractive. With an annual (2019–2020) output of LF slag of about 5 MT in China, this waste could, under 80 °C hydrothermal pretreatment, capture about 0.67 MT CO_2 if the mineral carbonation process is applied in steel plants.

Table 6. Comparison of current with previous steelmaking slag carbonation studies conducted under ambient temperature and pressure.

Slag Type	CO_2 Uptake (g of CO_2/1 kg of Slag)	Conditions	Reference
Al-rich LF slag	136.6	Temperature: 40 °C S/W ratio: 1:10 Reaction time: 1 h	This study

Table 6. *Cont.*

Slag Type	CO_2 Uptake (g of CO_2/1 kg of Slag)	Conditions	Reference
EAF steel slag	87	Temperature: 20 °C S/W ratio: 1:10 Reaction time: 37 min	[23]
BOF steel slag	116.4	Temperature: 70 °C S/W ratio: 1:2 Reaction time: 2 h	[24]
LF slag	67	Temperature: 20 °C S/W ratio: 1:20 Reaction time: 1 h	[25]
BOF steel slag	168.32	Temperature: 60 °C S/W ratio: 1:30 Reaction time: 10 h	[26]
LF slag	56	Temperature: 20 °C S/W ratio: 1:5 Reaction time: 70 min	[27]
BOF steel slag	215	Temperature: 60 °C S/W ratio: 1:5 Reaction time: 3 h	[28]

4. Conclusions

This study investigated the temperature of hydrothermal pretreatment on the hydrate formation and carbonation efficiency of Al-rich LF slag at ambient temperature and pressure. The main results are as follows:

During hydrothermal pretreatment, cubic C_3AH_6 was a main hydration product for 40 °C, 80 °C, and 100 °C-pretreated slags while $C_4A\overline{C}H_{11}$ and C_3AH_x with flaked shapes were the main hydrates for 20 °C and 80 °C-pretreated slags, respectively. Rhombohedral-shaped $CaCO_3$ was generated by the reaction between $C_{12}A_7$ in the slag and CO_2 in the air; and then $CaCO_3$ reacted with C_3AH_6 to form flake-shaped CCA. Flake-shaped products presented higher BET specific surface area. In 40 °C, 60 °C, and 100 °C-pretreated slags, a dense $CaCO_3$ layer surrounded the unreacted core of the slag particle, resulting in the hindrance of further $C_{12}A_7$ hydration.

Flake-shaped products could provide a lager reaction surface area and avoid the calcite and AH gel layer formation on the surface of the unreacted hydrates. Therefore, 80 °C and 20 °C-pretreated slags containing a larger number of flake-shaped hydrates had larger CO_2 uptake (13.66 wt% and 10.82 wt%, respectively). Cubic C_3AH_6 crystal and unhydrated raw slag particles were less inactive for carbonation, resulting in the smaller CO_2 uptake for 40 °C, 60 °C, and 100 °C-pretreated slags (9.21 wt%, 9.83 wt% and 6.84 wt%, respectively). In short, the carbonation efficiency of the pretreated slag was strongly associated with the morphology of the hydration products and the hydration extent of LF slag.

Author Contributions: Investigation, Y.H.; resources, G.X.; writing—original draft preparation, G.X.; writing—review and editing, Y.H.; supervision, G.X.; funding acquisition, Y.H. Both authors have read and agreed to the published version of the manuscript.

Funding: This work was funded by the Natural Science Foundation of Hunan Province, China (Grant No. 2020JJ4157).

Data Availability Statement: The data presented in this study are available on request from the corresponding author. The data are not publicly available due to patent issues.

Acknowledgments: The authors thank the support from the Research Foundation of the Natural Science Foundation of Hunan Province, China (Grant No. 2020JJ4157).

Conflicts of Interest: The authors declare no conflict of interest.

References

1. International Energy Agency. *Global Energy & CO_2 Status Report: The Latest Trends in 2018*; International Energy Agency: Pairs, France, 2019.
2. Sun, Y.; Yao, M.S.; Zhang, J.P.; Yang, G. Indirect CO_2 mineral sequestration by steelmaking slag with NH_4Cl as leaching solution. *Chem. Eng. J.* **2011**, *173*, 437–445. [CrossRef]
3. Rushendra Revathy, T.D.; Palanivelu, K. Direct mineral carbonation of steelmaking slag for CO_2 sequestration at room temperature. *Environ. Sci. Pollut. Res.* **2016**, *23*, 7349–7359. [CrossRef] [PubMed]
4. Liu, W.Z.; Yin, S.; Luo, D.M.; Zhang, G.Q.; Yue, H.R.; Liang, B.; Wang, L.M.; Li, C. Optimizing the recovery of high-value-added ammonium alum during mineral carbonation of blast furnace slag. *J. Alloys Compd.* **2019**, *774*, 1151–1159. [CrossRef]
5. Rushendra Revathy, T.D.; Ramachandran, A.; Palanivelu, K. Sequestration of CO_2 by red mud with flue gas using response surface methodology. *Carbon Manag.* **2021**, *12*, 139–151. [CrossRef]
6. Wang, Y.J.; Zeng, Y.N.; Li, J.G.; Zhang, Y.Z.; Zhao, Q.Z. Carbonation of argon oxygen decarburization stainless steel slag and its effect on chromium leachability. *J. Clean. Prod.* **2020**, *256*, 120377. [CrossRef]
7. Ho, H.J.; Lizuka, A.; Shibata, E. Utilization of low-calcium fly ash via direct aqueous carbonation with a low-energy input: Determination of carbonation reaction and evaluation of the potential for CO_2 sequestration and utilization. *J. Waste Manag.* **2021**, *288*, 112411.
8. Liu, W.; Teng, L.; Rohani, S.; Qin, Z.; Zhao, B.; Xu, C.C.; Ren, S.; Liu, Q.; Liang, B. CO_2 mineral carbonation using industrial solid wastes: A review of recent developments. *J. Chem. Eng.* **2021**, *416*, 129093. [CrossRef]
9. Ibrahim, M.H.; El-Naas, M.H.; Benamor, A.; Al-Sobhi, S.S.; Zhang, Z. Carbon mineralization by reaction with steel-making waste: A review. *Processes* **2019**, *7*, 115. [CrossRef]
10. Santos, R.M.; François, D.; Mertrn, G.; Elsen, J.; Gerven, T.V. Ultrasound-enhanced mineral carbonation. *Appl. Therm. Eng.* **2013**, *157*, 109–116.
11. Huang, Y.; Zeng, Z. Improvement of desulfurization efficiency of Al-rich ladle furnace refining slag with an aqueous carbonation method by hydrothermal or ultrasound pretreatment. *Environ. Sci. Pollut. Res.* **2021**, *28*, 27703–27711. [CrossRef]
12. Koplík, J.; Tomala, L.; Novotný, R. Hydration of calcium aluminate phases at different temperatures. *Adv. Mater. Res.* **2014**, *1000*, 24–27. [CrossRef]
13. Edmonds, R.N.; Majumdar, A.J. The hydration of $12CaO.7Al_2O_3$ at different temperatures. *Cem. Concr. Res.* **1988**, *18*, 473–478. [CrossRef]
14. El-Naas, M.H.; Maisa, E.G.; Hameedi, S.; Mohamed, A.-M.O. CO_2 sequestration using accelerated gas-solid carbonation of pre-treated EAF steel-making bag house dust. *J. Environ. Manag.* **2015**, *156*, 218–224.
15. Wang, Z.P.; Yang, H.Y.; Zhao, Y.T.; Lu, L.L.; Jia, D.L. Delaying Effect of NaCl on the conversion of hydrates of calcium aluminate cement. In Proceedings of the 11th International Conference on High-Performance Ceramics, Kunming, China, 25–29 May 2019.
16. Ewa, L.; Dominika, M. Structure, microstructure and thermal stability characterizations of C_3AH_6 synthesized from different precursors through hydration. *J. Therm. Anal. Calorim.* **2020**, *139*, 1693–1706.
17. Liu, W.; Zhang, H.; Zhou, Q.S.; Peng, Z.H.; Qi, T.G.; Li, X.B.; Liu, G.H. Reaction tricalcium aluminate hexahydrate(C_3AH_6) with carbon dioxide. *J. Cent. South Univ.* **2011**, *42*, 595–598.
18. Xiao, J.; Gou, F.; Jin, Y.G.; Wang, Y.H. Effect of $CaCO_3$ on hydration characteristics of C_3A. *J. Cent. South Univ. Technol.* **2010**, *17*, 918–923. [CrossRef]
19. Luz, A.P.; Pandolfelli, V.C. $CaCO_3$ addition effect on the hydration and mechanical strength evolution of calcium aluminate cement for endodontic applications. *Ceram. Int.* **2012**, *38*, 1417–1425. [CrossRef]
20. Feng, Y.B.; Tang, C.M.; Qiu, T. Effect of ball milling and moderate surface oxidization on the microwave absorption properties of FeSiAl composites. *Mater. Sci. Eng. B* **2013**, *178*, 1005–1011. [CrossRef]
21. Sun, Y.; Yang, G.; Li, K.; Zhang, L.C.; Zhang, L. CO_2 mineralization using basic oxygen furnace slag: Process optimization by response surface methodology. *Environ. Earth. Sci.* **2016**, *75*, 1335. [CrossRef]
22. Yi, Y.R.; Han, M.F. The reactivity of carbon dioxide capture with calcium-based waste solid by wet process. *J. China Coal Soc.* **2012**, *37*, 1205–1210.
23. Uibu, M.; Kuusik, R.; Andreas, L.; Kirsimäe, K. The CO_2-binding by Ca–Mgsilicates in direct aqueous carbonation of oil shale ash and steel slag. *Energy Procedia* **2011**, *4*, 925–932. [CrossRef]
24. Wang, C.Y.; Bao, W.J.; Guo, Z.C.; Li, H.Q. Carbon Dioxide Sequestration via Steelmaking Slag Carbonation in Alkali Solutions: Experimental Investigation and Process Evaluation. *Acta Metall. Sinica* **2018**, *31*, 771–784. [CrossRef]
25. Paris, K.A.; Hills, C.D.; Maries, A.; Gunning, P.J.; Wray, D.S. Enhancement of accelerated carbonation of alkaline waste residues.by ultrasound. *Waste Manag.* **2016**, *50*, 121–129.
26. Chen, Z.M.; Li, R.; Zheng, X.M.; Liu, J.X. Carbon sequestration of steel slag and carbonation for activating RO phase. *Cem. Concr. Res.* **2021**, *139*, 106271. [CrossRef]
27. Yi, Y.R.; Lin, Y.; Du, Y.C.; Bai, S.Q.; Ma, Z.L.; Chen, Y.G. Accelerated carbonation of ladle furnace slag and characterization of its mineral phase. *Cem. Concr. Res.* **2021**, *276*, 122235.
28. Chen, K.W.; Pan, S.Y.; Chen, C.T.; Chen, Y.H.; Qiang, R.C. High-gravity carbonation of basic oxygen furnace slag for CO_2 fixation and utilization in blended cement. *J. Cleaner Prod.* **2016**, *124*, 350–360. [CrossRef]